ACS OMEGA

Open Access

http://pubs.acs.org/journal/acsodf

Article

Affordable Two-Dimensional Layered Cd(II) Coordination Polymer: High-Performance Pseudocapacitor Electrode Behavior

Samika Anand, Sunaja Devi Kalathiparambil Rajendra Pai,* Abhishek Kumar, and Channabasaveshwar V. Yelamaggad*

Cite This: *ACS Omega* 2024, 9, 41807−41818

Read Online

ACCESS | Metrics & More | Article Recommendations | Supporting Information

ABSTRACT: In recent years, pseudocapacitive materials have been investigated rigorously as they provide a unique pathway for realizing high-energy and high-power densities. However, innovative approaches involving rational design and synthesis of new materials are still vital to address concerns such as degradation, low conductivity, low cycling performance, high resistance, production cost, etc. Working in this direction, we report the cost-effective synthesis, characterization, and excellent pseudocapacitive behavior of a Cd(II)-based coordination polymer (COP) abbreviated as Cd(DAB). It has been realized in quantitative yield through a facile one-pot reaction occurring among the N4-ligand, 3,3′-diaminobenzidine (DAB), and Cd(II) ions, derived from $Cd(OAc)_2{\cdot}2H_2O$, at room temperature. The proposed structure of the COP was ascertained by subjecting it to various standard spectroscopic and electron microscopic studies; these techniques reveal the self-assembly of indefinitely long coordination strands into a two-dimensional (2D) layered structure. The electrochemical performance of Cd(DAB) was evaluated as an electrode material for supercapacitors. Owing to its high conductivity, it portrayed remarkable energy storage (pseudocapacitor) behavior; it exhibited a high specific capacitance of 1341.6 F g^{-1} and a long cycle life with 81% retention over 10,000 cycles at 20 A g^{-1}. Additionally, an asymmetrical supercapacitor device was fabricated, which exhibited a specific capacitance of 428.5 F g^{-1} at a current density of 1 A g^{-1}.

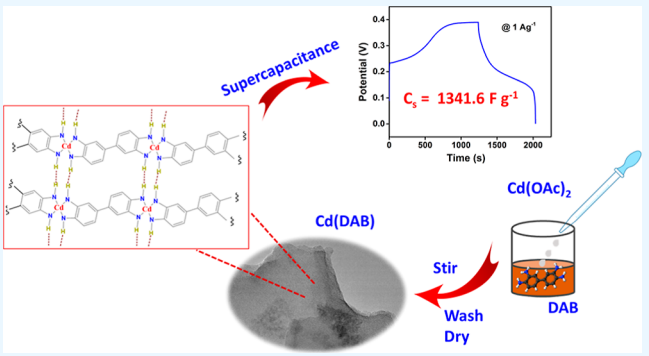

INTRODUCTION

Energy consumption across the globe has been increasing progressively, resulting in an energy crisis. Given that the supply of energy from fossil fuels is challenging and unsustainable (limited), several investigations on reliable and low-cost functional materials for energy applications have been undertaken in recent years. A wide range of materials for rechargeable batteries, thermoelectric applications, fuel cells, photovoltaics, semiconducting devices, etc., have been explored to address energy concerns. In particular, advanced materials capable of serving as active media in storing, transporting, or converting them into other forms of energy have been actively considered for both fundamental research and practical applications.[1−4] Under the theme/category of harvesting energy from renewable sources, the materials required for energy storage devices, especially supercapacitors (SCs), have been attracting a great deal of attention because of their promising characteristics such as long life, fast charge/discharge rates, high-specific capacity/power density, affordability, eco-friendliness, eco-compatibility, etc. Notably, they are not only used as independent/direct power sources but can also be conjugated with batteries. Given these features, they have been used in portable devices, electric vehicles, and grid energy storage; specifically, their usage in electric vehicles is becoming inevitable.[5] Most importantly, the electrochemical performance of the SCs, especially the capacitive behavior, is dependent largely on the choice of electrode materials. As is well-known, based on the charge storage process, SCs can be classified into three categories: (I) electric double-layer capacitors (EDLCs), (II) pseudocapacitors, and (III) hybrid SCs. As shown in Figure 1, EDLCs use double-layer electrodes to store charge electrostatically (Figure 1a), pseudocapacitors store charge faradaically via a redox mechanism involving the transfer of charge between electrodes and electrolytes (Figure 1b), and hybrid SCs store charge via a combination of faradaic and nonfaradaic processes (Figure 1c). Over the past three decades or so, a wide range of functional materials have been explored with the prime objective of improving their overall (capacitive) behavior.[6−8] The investigated electrode materials

Received: July 3, 2024
Revised: August 5, 2024
Accepted: August 27, 2024
Published: September 20, 2024

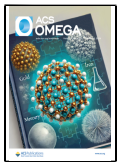

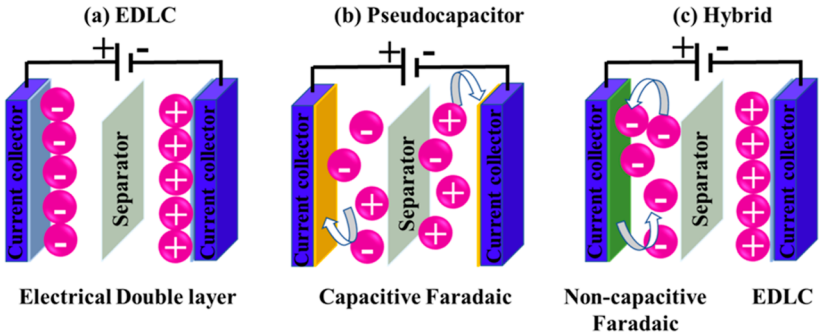

Figure 1. Schematic presentation showing the charge storage processes in (a) EDLCs, (b) pseudocapacitors, and (c) hybrid SCs.

for SCs include conducting polymers, two-dimensional (2D) motifs, metal oxide/hydroxide-based materials, carbon-based materials, etc. Of these, coordination polymers (COPs) appear to be most promising.

COPs make up a class of functional materials that consist of metal ions bonded to repetitive organic ligands through coordinate bonds. These materials have gained substantial attention owing to their diverse range of properties and potential applications. These highly ordered and porous materials are composed of metal nodes (often transition metal ions) connected by organic ligands.[15] The metal−ligand coordination bonds serve as the structural components that hold the infinite network together. The organic ligands used in COPs typically comprise functional groups like carboxylates, pyridines, or imidazoles.[9−11] These ligands serve as linkers between metal nodes, creating a one-dimensional (1D) chain that may undergo self-assembly due to secondary interactions like hydrogen bonding, $\pi-\pi$ stacking, dipole−dipole, and van der Waals interactions, giving rise to 2D sheets or 3D frameworks.[11,12] COPs can exhibit diverse structures and topologies depending on the choice of metal ions and ligands. This diversity allows for tailoring these materials for specific applications. COPs have been studied for their increased surface area, permanent porosity, adsorption affinity, and optical and magnetic properties over the years.[13] These characteristics render them appropriate for gas storage,[14,15] energy storage,[16] drug delivery,[17] catalysis,[18,19] conductivity studies,[20] and sensing.[21,22]

Transition metal-based COPs have been a subject of extensive research and development. They offer a wide range of coordination numbers, oxidation states, and coordination geometries, making them highly versatile for the design and synthesis of COPs. This diversity allows researchers to create a broad spectrum of materials with various properties and functions. Owing to a rich palette of redox-active sites and unique electronic configurations offered by these metals, transition metal-based COPs can emerge as ideal candidates for applications ranging from electrocatalysis and energy storage to photovoltaics and fuel cells. Recent advancements in Co-based, Mn-based, and Ni-based COPs highlight their potential applications in pseudocapacitors due to their reversible Faradaic redox reactions, which enhance energy density, power density, and cycling stability.[23−27] The incorporation of redox-active metal centers within the COP array opens avenues for efficient charge transfer, making these materials particularly attractive for energy storage applications.[28,29] While COPs based on transition metals have been reported, their electrochemical properties have rarely been investigated. It has been reported that a number of COPs have lower specific capacities due to their intricate synthetic processes.

In continuation of research endeavors in this direction,[16] we developed a Cd(II)-based COP involving 3,3′-diaminobenzidine (DAB) as the ligand and examined its electrochemical (energy storage) behavior. Here, we describe the facile synthesis and characterization of COP, abbreviated Cd(DAB), and discuss its potential application as an electrode material for pseudocapacitors. The choice of Cd as the central metal in COP is motivated by its intriguing electronic structure and potential for facilitating efficient charge storage.

MATERIALS AND METHODS

Materials. All chemicals were utilized without modification. Analytical-grade solvents obtained from Merck were dried using customary protocols before use. DAB was obtained from TCI Chemicals, whereas polyvinylidene fluoride (PVDF), *N*-methyl-2-pyrrolidone (NMP), and cadmium acetate dihydrate ($Cd(OAc)_2\times 2H_2O$) were obtained from Sigma-Aldrich.

Characterization Techniques. To confirm the formation of Cd(DAB), X-ray diffraction (XRD) was carried out using a Rigaku SmartLab X-ray diffractometer equipped with Cu Kα radiation. The Raman spectroscopic data were obtained using a Raman spectroscope with 532 nm excitation (Horiba Jobin Yvon XploRA PLUS V1.2 MULTILINE). The FTIR spectra were obtained using a PerkinElmer Spectrum 1000 FT-IR spectrometer. X-ray photoelectron spectroscopy (XPS) was utilized to perform elemental and compositional analysis. Kratos X-ray photoelectron spectrometer Axis Ultra DLD was used to obtain the spectroscopic data. The structural, morphological, and compositional analysis of the COP was carried out using field emission scanning electron microscopy (FESEM) with energy-dispersive spectrometry (EDS) and confirmed by high-resolution transmission electron microscopy (HRTEM), employing a Carl Zeiss Supra 55 and Thermo Fisher Scientific Talos F200S G2, respectively. Thermal stability was evaluated using thermogravimetric analysis (TGA) employing NETZSCH STA 2000.

Preparation of Cd(DAB). The new COP, Cd(DAB), was synthesized by a modified method under ambient conditions.[16,49] An aqueous solution of the metal precursor, $Cd(OAc)_2\cdot 2H_2O$, (1.33 g, 5 mmol), was added to an ethanolic dispersion of DAB (1.074 g, 5 mmol), and the mixture was stirred at room temperature for 10 min. The precipitate obtained was filtered and washed multiple times with warm water and ethanol, followed by heating in ethanol. The precipitate was centrifuged with multiple washings using water and ethanol. It was dried overnight at 60 °C, when COP was obtained as a dark brown free flowing powder. Figure 2

https://doi.org/10.1021/acsomega.4c06108
ACS Omega 2024, 9, 41807−41818

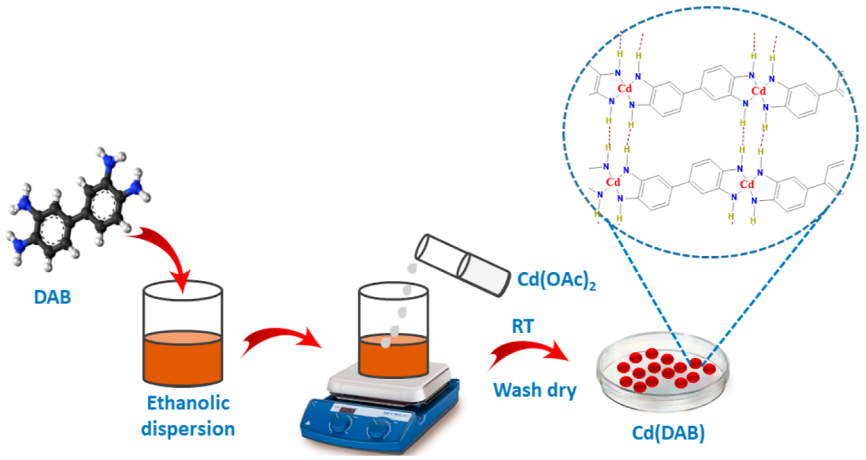

Figure 2. Schematic representation for the synthesis of Cd(DAB).

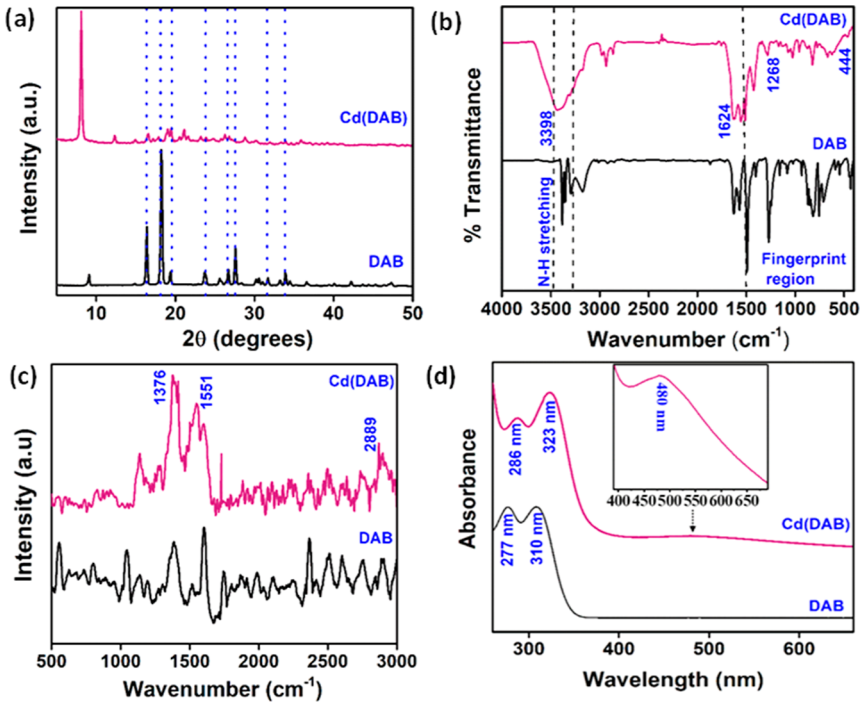

Figure 3. (a) X-ray diffractograms, (b) FTIR spectra, (c) Raman spectra, and (d) UV−vis spectra.

pictorially depicts the procedure followed for the synthesis of Cd(DAB).

Electrochemical Measurements. A CHI608E electrochemical workstation (CH Instruments Inc. USA) with a three-electrode system was utilized for electrochemical investigations. Supercapacitance measurements were carried out with calomel as the reference electrode, Pt wire as the counter electrode, and the prepared sample coated on Ni foam as the working electrode using 3 M KOH as the electrolyte. The working electrode was prepared by drop casting an aqueous slurry of the sample, which was prepared by mixing the COP (1.5 g) with activated carbon (0.289 g), 0.0938 g of PVDF, and 60 μL of NMP on Ni foam and drying it overnight. Cyclic voltammetry (CV), galvanostatic charge/discharge (GCD), and electrochemical impedance spectroscopy (EIS) were the techniques used to evaluate the supercapacitance behavior of the prepared sample at room temperature. The specific capacitance (C_s), energy density (E), and power density (P) were obtained using eqs 1−3, respectively.

$$\mathrm{Cs} = \frac{I \times \Delta t}{m \times V} \tag{1}$$

$$E = \frac{1}{2} \times \frac{\mathrm{Cs} \times V^2}{3.6} \tag{2}$$

$$P = \frac{E \times 3600}{\Delta t} \tag{3}$$

RESULTS AND DISCUSSION

Characterization of Cd(DAB). The XRD patterns obtained for both DAB (ligand) and COP, Cd(DAB), are depicted in Figure 3a. The intense peaks of DAB observed at 2θ = 16.2, 18.2, 19.6, 23.8, 26.7, 27.8, 31.6, and 33.9° (Figure 3a, black-trace) correspond to (011), (−111), (111), (020),

https://doi.org/10.1021/acsomega.4c06108
ACS Omega 2024, 9, 41807−41818

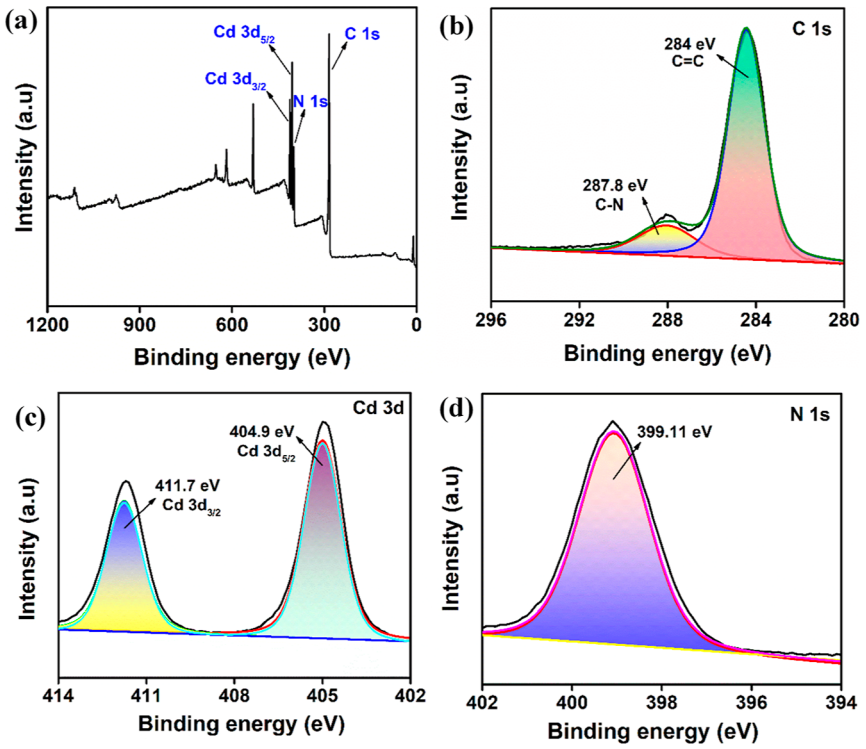

Figure 4. XPS survey spectrum of (a) Cd(DAB). High-resolution XPS spectrum of (b) C 1s, (c) Cd 3d, and (d) N 1s.

(−112), (−121), (−221), and (−122), respectively.[16] As compared to the XRD pattern of the DAB, the profile of Cd(DAB) shows a significant decrease in peak intensity (Figure 3a, maroon-trace), pointing toward the formation of a COP. However, the first peak at 8.99° of the profile, which is the most prominent diffraction peak, is indicative of ordered and regularly spaced atomic arrangements. As can be seen, the diffractogram comprises the reflections of peaks from the DAB segment with a slight shift in planes, indicating the presence of mild strain effects in the crystal lattice. The absence of peaks at 46.2 and 53.1° (JCPDS card no 05-0640) eliminates the possibility of the presence of CdO[30] or any unreacted precursors.

Figure 3b (black and maroon traces) shows the FTIR spectra of both the ligand and COP. The FTIR spectrum of Cd(DAB) (Figure 3b, maroon trace) appears to be significantly different from that of DAB, especially in the fingerprint region (1500−400 cm^{-1}). The presence of a peak at 444 cm^{-1} points toward Cd−N stretching vibration, which is indicative of the formation of a metal−ligand coordinate bond with N as the donor site.[31] The vibrational peak at 1268 cm^{-1} indicates C−N stretching, whereas the one seen at 1624 cm^{-1} indicates C−C stretching vibrations.[32] The broad peak at ∼3350 cm^{-1} suggests N−H stretching vibrations. Two sharp peaks at 3350 and 3385 cm^{-1} indicate free amine N−H stretching vibrations in DAB (Figure 3b, black trace); the broadening of this peak after complexation provides evidence of the association of nitrogen with metal ions of Cd(DAB) and DAB.

As can be seen in Figure 3c (maroon trace), the Raman spectrum of the COP does not resemble the ligand spectrum (black trace). The spectrum of Cd(DAB) possesses two intense bands at 1376 and 1551 cm^{-1}. These bands obtained are similar to the D and G bands of graphitic (2D) materials, typically observed at 1360 and 1560 cm^{-1}, respectively. The G band in graphitic materials arises as a result of C−C stretching, a signature of the sp^2 carbons.[33] The occurrence of the D band is attributed to the breathing modes of sp^2 carbon atoms; it is a double resonance band that originates due to a 1-phonon lattice vibrational process.[34] These findings suggest the 2D structure for the COP synthesized.[35] As we shall discuss later, this assumption is substantiated by the FESEM and HRTEM images.

The occurrence of a broad band at 2889 cm^{-1} suggests the presence of multiple stacked layers in the COP. Figure 3d, with maroon and black traces, shows the UV−vis spectra of the COP, Cd(DAB), and ligand, DAB. The UV−vis profile of the ligand comprises two equally intense peaks located at ∼277 and ∼310 nm (Figure 3, black trace) arising, respectively, due to the $\pi \rightarrow \pi^*$ and $n \rightarrow \pi^*$ transitions in DAB. It is immediately apparent that the spectrum of COP shows similar peaks but with a notable red shift; i.e., they exist at ∼286 and ∼323 nm (Figure 3d, maroon trace). This bathochromic shift of the peaks not only serves as evidence for extended π-conjugation in the COP but also indicates an internal charge transfer occurring between Cd^{2+} and DAB.[36] This, along with the hydrogen (H)-bonds existing between the indefinitely long strands to form 2D COP sheets, may be another possible reason for the observed red shift.[37] A broad band centered around 480 nm can be additionally seen (Figure 3d-inset). Although presently, we do not have a precise idea about the origin of the peak, but it might have arisen from the charged species formed by the complex when it comes in contact with the solvent molecules.[38]

The COP was examined with the aid of XPS to determine the chemical state of the elements and the composition of the materials. The XPS survey spectrum obtained is shown in Figure 4a. The peaks at 285.9, 399.11, 404.9, and 411.7 eV, on the survey scan, correspond to C 1s, N 1s, Cd $3d_{5/2}$, and Cd $3d_{3/2}$, respectively. The atomic percentage (at. %) of C 1s, N

https://doi.org/10.1021/acsomega.4c06108
ACS Omega 2024, 9, 41807−41818

1s, Cd $3d_{5/2}$, and Cd $3d_{3/2}$, as obtained from the survey spectrum, was found to be 77.94, 16.96, 2.81, and 2.83%, respectively. The survey spectrum analysis is consolidated in Table 1. Further information about the elements present and their chemical state, as well as their chemical (bonding) surroundings, was provided by a high-resolution scan for each peak. The individual spectra for C 1s, Cd 3d, and N 1s are shown in Figure 4, respectively, and their peak analysis is summarized in Table 2. As shown in Figure 4b, there are two distinct binding energies of C 1s electrons that can be attributed to two different chemical environments. The peak at 284 eV corresponds to sp^2-hybridized carbon in the aromatic ring (C═C), whereas the other band seen at 287.8 eV belongs to sp^2-hybridized C linked to N.[39] The C−N binding energy appears to be slightly greater than the typical value of 285.3 eV. The increase in binding energy, nearly close to that of C═N (287.6 eV), may be ascribed to the long-range delocalization of electrons in the polymeric strand, resulting in a partial double bond character of the C−N bond.[40] Two peaks in the Cd(II) spectra (Figure 4c) at 411.7 and 404.9 eV can be attributed to Cd $3d_{3/2}$ and Cd $3d_{5/2}$, respectively.[41] A single peak at 399.11 eV in the N 1s spectrum (Figure 4d) suggests that N is present in a single oxidation state/chemical environment.[42,43]

Table 1. XPS Survey Spectrum Analysis for Cd (DAB)

Binding energy (eV)	Element	Atomic %
285.9	C 1s	77.94
399.1	N 1s	16.96
404.9	Cd $3d_{5/2}$	2.83
411.7	Cd $3d_{3/2}$	2.81

Table 2. XPS Peak Analysis for Cd (DAB)

High-resolution spectra	Binding energy (eV)	Bonding
C 1s	284.0	C═C
	287.8	C−N
Cd 3d	404.9	Cd $3d_{5/2}$
	411.7	Cd $3d_{3/2}$
N 1s	399.1	C−NH

As is known, Cd(II) has a d^{10} electronic configuration, which allows it to adopt coordination numbers ranging from 2 to 9. According to previous literature reports, four coordinate complexes of Cd(II) are particularly common due to favorable geometry and stability.[44] FTIR and Raman spectroscopic studies of $[Cd(NH_3)_4]^{2+}$ and $[Cd(NH_3)_6]^{2+}$ have proved the increase in binding strength between metal ion and ligand with lowering of the coordination number.[45] Zhai et al. reported Cd(datrz)I, (datrz = 3,5-diamino-1,2,4-triazole), a two-dimensional COP where Cd(II) showed N-4 interaction with N donor sites from datrz.[46] Owing to the coordination environment (coordination number 4) of Cd(II), the possibility of $\pi-\pi$, M−π, and M−M interactions in the COP was discarded. This was in line with the structure of Cd(DAB) obtained in the

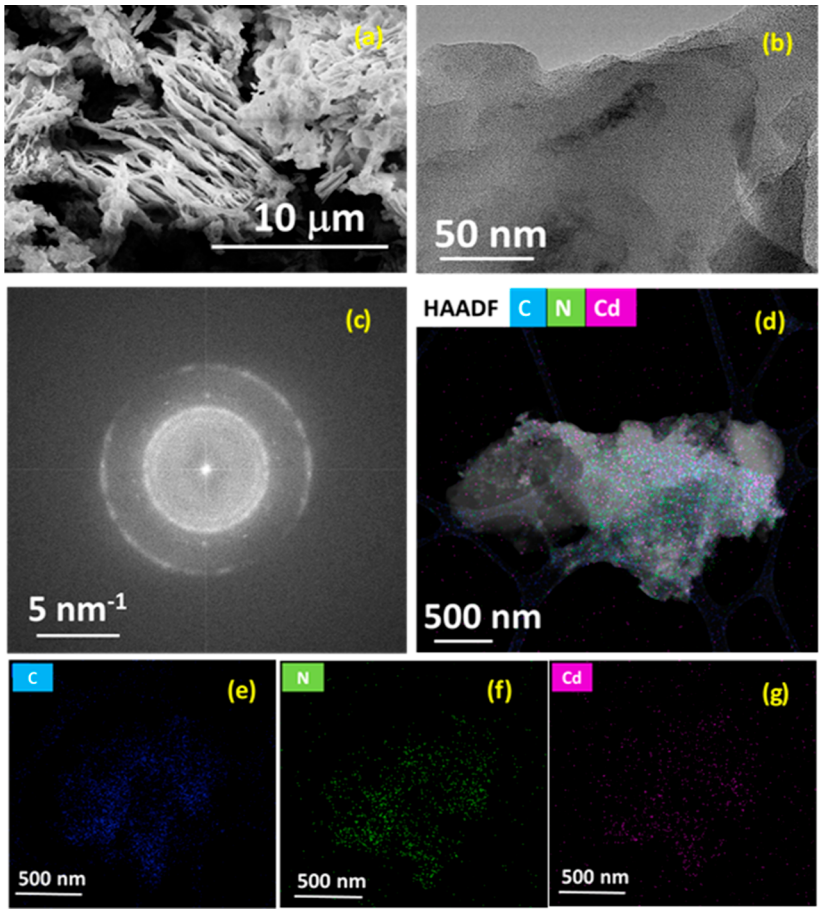

Figure 5. (a) FESEM image, (b) HRTEM image, (c) SAED pattern, (d) HAADF−STEM image of Cd(DAB), and (e−g) elemental mapping of C, N, and Cd.

https://doi.org/10.1021/acsomega.4c06108
ACS Omega 2024, 9, 41807−41818

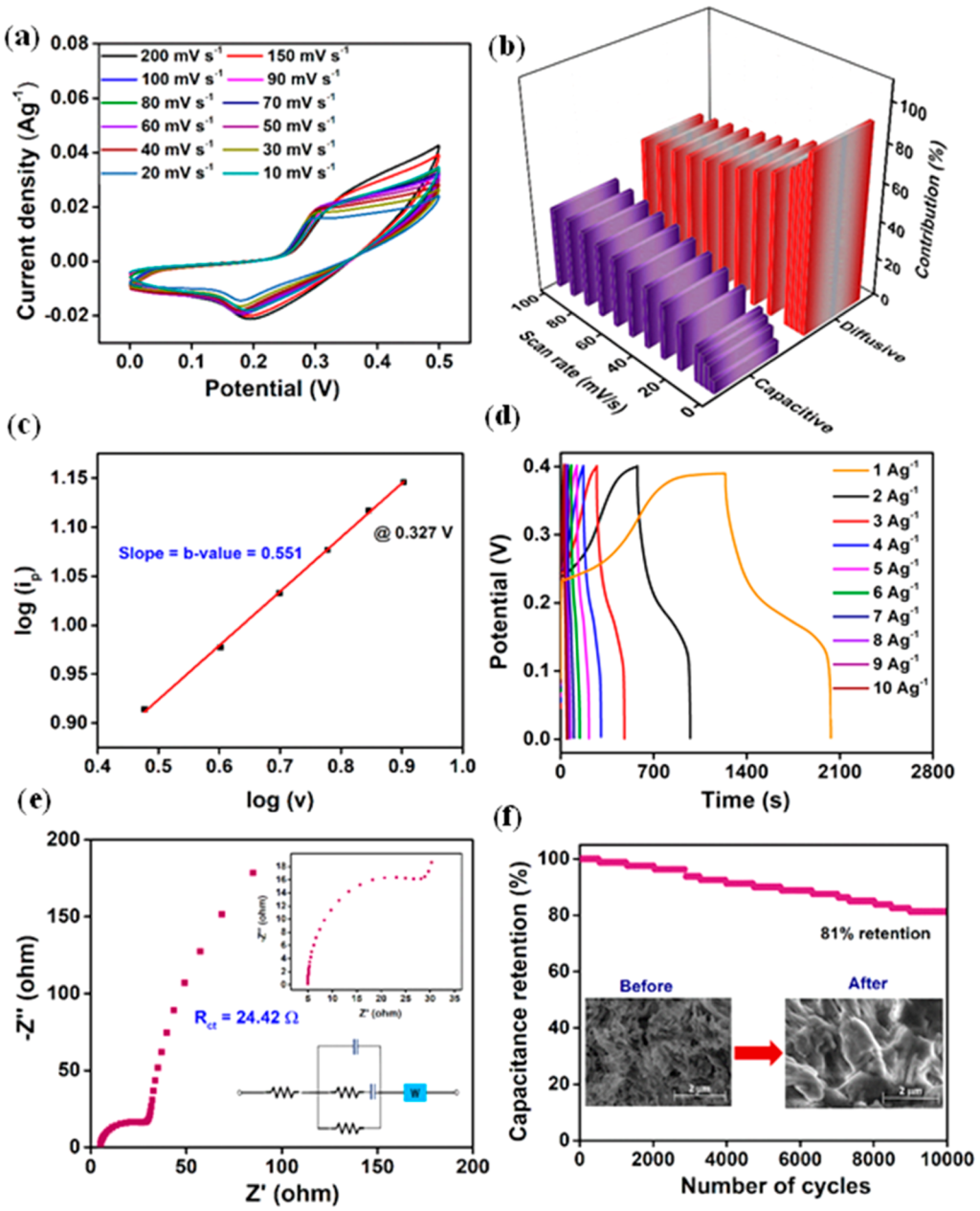

Figure 6. (a) Cyclic voltammograms of Cd(DAB) at various scan rates, (b) GCD curves at different current densities, (c) representation of capacitive and diffusive contributions at different scan rates, (d) linear plot of log(i_p) vs log(v), (e) Nyquist plot, and (f) cyclic stability of Cd(DAB) at a current density of 20 A g^{-1} using a three-electrode system.

present case, where the layered COP was formed due to self-assembly (hydrogen bonding) between one-dimensional long polymeric chains. The size, shape, and electronic property of the Cd(II) ion and the ligand involved may favor tetrahedral coordination in the present case.[47] Tetrahedral coordination allows for optimal spacing between the relatively large Cd(II) ions and the ligand DAB, minimizing steric hindrance and maximizing stability. In addition to numerous experimental observations, including those conducted by ourselves and other researchers, which have contributed to our understanding of the structural elucidation of analogous systems, we utilized this knowledge to predict and confirm the neutral structure of the novel complex described in our study.[48,49] Extensive literature review further supports our assertion, indicating that previously reported complexes of a similar nature are indeed neutral, with C−N bonds exhibiting double-bond characteristics.[50−53] It is well-established that during the formation of metal complexes in solution, particularly when water is employed as a solvent, significant changes occur in enthalpy and entropy characteristics. Initially, there is a decrease in the enthalpy, facilitating the association of inherently unstable metal ions with small ligands, such as solvent molecules, to form coordination complexes. Subsequently, as coordination bonds form, these small ligands are completely substituted by larger ligands, resulting in a decrease in entropy due to the release of smaller molecules/ligands. However, smaller molecules may remain associated with the metal cations if the coordination numbers/sites are not fully occupied by the larger ligands (in the case of lanthanides). In cases where multidentate ligands participate in coordination,

https://doi.org/10.1021/acsomega.4c06108
ACS Omega 2024, 9, 41807−41818

the increase in entropy is more probable, as the bringing together of two molecules entails less entropy cost than interactions among three or more molecules. Consequently, a majority of coordination reactions occur spontaneously and are enthalpically and/or entropically favored.[54−57]

FESEM was employed to obtain images and reveal the detailed surface information of samples. Figure 5a shows the FESEM image of the prepared COP, Cd(DAB). The image indicates that Cd(DAB) possesses thin planar 2D layers stacked on top of each other. These thin, sheet-like structures, having smooth surfaces, associate with each other to yield thick bundles. As discussed earlier, the planar 2D sheets /layers are formed by the self-assembly (association) of indefinitely long COP strands formed through H-bonds. Furthermore, the energy-dispersive X-ray spectroscopy (EDS) technique was utilized to examine the elemental composition of COP realized. The weight (wt) percentage (%) of elements, viz., C, N, and Cd, could be figured out by this technique. The EDS spectrum depicted in Figure S1a,b indicated the occurrence of elements C, N, and Cd in 34.32, 27.35, and 38.33 wt %, respectively. The elemental mapping, shown in Figure S1c−e, also illustrated the uniform distribution of C, N, and Cd elements over the proposed layered structure. HRTEM was used to examine the crystallographic structure of the COP. The HRTEM image shown in Figure 5b supports the interpretation of the FESEM study that the synthesized COP has planar 2D sheets bundled together over a large scale. The polycrystalline character of the COP was further confirmed by carrying out a SAED (selected area electron diffraction) experiment; the diffraction pattern obtained has been presented in Figure 5c. To map the elements of the Cd(DAB), high-angle annular dark-field scanning transmission electron microscopy imaging was used. Figure 5d displays the HAADF−STEM image together with the elemental mapping for the C, Cd, and N elements (Figure 5e−g). The mapping illustrates the distribution of elements across the proposed layered 2D structure.

The as-synthesized COP was evaluated for its thermal stability using TGA. The thermogram of Cd(DAB), depicted in Figure S2, revealed that the polymeric material particularly showed two weight loss regions, stage 1 from 150 to 300 °C and stage 2 from 300 to 700 °C. A weight loss of 19.9% in stage 1 may be ascribed to the partial disintegration of polymeric framework due to breaking of H-bonds connecting 1D strands. Major weight loss of 54.6% observed in stage 2 is attributed to the decomposition of DAB moieties, leaving a residual mass of 25.4%.

Electrochemical Properties of Cd(DAB). It is clear from the discussion presented above that the Cd(II)-based COP synthesized in this study is a 2D material featuring repetitive metal nodes and organic ligands bound to each other through coordination bonds. As is known, the combination of two-dimensionality and coordination networks endows the material with several physicochemical characteristics. The framework is expected to exhibit high electric conductivity due to the extended π conjugation on the ligands across the metal ion centers. The redox behavior with multielectron transfer should be the prime characteristic of such systems. Given these promising features, these 2D frameworks (materials) should have the ability to store energy through a multielectron transfer in a rechargeable device. Thus, the electrochemical behavior of the newly synthesized COP was studied by using a conventional three-electrode cell configuration by CV, GCD experiments, and EIS investigations.

Figure 6a depicts the cyclic voltammograms of Cd(DAB) obtained within the potential window 0−0.5 V, with scan rates changing from 200 to 10 mV s^{-1}. The CV at 10 mV s^{-1} (Figure S3a) displays two peaks at 0.177 and 0.292 V, corresponding to cathodic reduction and anodic oxidation, respectively. Figure S3b also depicts the CV curve of the working electrode in comparison with that of bare Ni foam (at 10 mV s^{-1}), evidencing the negligible contribution of Ni foam toward redox behavior. The curves show two distinct characteristics peaks comprising faradic contributions from the redox reactions, thereby suggesting the pseudocapacitive nature of the material. The redox peaks appear to be well defined with negligible contribution from double-layer capacitance. The nature of the two faradic peaks is indicative of intercalation pseudocapacitors, which is commonly observed for layered materials.[58] Owing to the intercalation−deintercalation process, the CV exhibits plateaus instead of sharp triangular peaks.[59] Intercalation pseudocapacitors have been known for rapid charge storage rates, outshining surface redox supercapacitive materials. The remarkable activity of such materials is ascribed to the intercalation of electrolyte ions within the layers of the COP with no phase transformation.[60,61] It has been noted that an increase in the scan rate is accompanied by an increase in current density, which exacerbates the area of the CV curve. This is explained by the fact that with greater scan speeds, the electrolyte's diffusion layer width decreases. Better specific capacity at higher scan rates is indicated by the increase in the curve area.

Further, the power law relationship (eq 4) was employed to elucidate the charge storage dynamics in Cd(DAB).

$$i_p = k_1 v + k_2 v^{1/2} \tag{4}$$

where i_p refers to the peak current at a particular potential and v is the scan rate in V/s; $k_1 v$ and $k_2 v^{1/2}$ are the surface capacitive and diffusive contribution, respectively. A graph between $\frac{i_p}{v^{1/2}}$ vs $v^{1/2}$ is plotted (at 0.327 V, here), where the slope and y-intercept from the linear fitting obtained are k_1 and k_2, respectively.[62] Figure S4a depicts the cyclic voltammograms recorded at lower scan rates (from 1 to 10 mV s^{-1}), which are well-known for power law calculations. In order to elucidate capacitive and diffusive current contributions, we chose a potential of 0.327 V, where a maximum current response was observed. Figure S4b depicts a plot of $\frac{i_p}{v^{1/2}}$ vs $v^{1/2}$ (at 0.327 V). From the linear fitting, the slope (k_1) and y-intercept (k_2) were obtained to be 0.30899 and 0.1305. Thus, these values in the power law relationship (eq 4) further aided in deciphering the capacitive ($k_1 v$) and diffusive ($k_2 v^{1/2}$) contributions at different scan rates. Figure 6b showcases a bar representation of the surface current contributions at different scan rates. The diffusion and capacitive current (%) at 1 mV s^{-1} was calculated to be 93.03 and 6.965%, respectively. It is clear that Cd(DAB) demonstrates greater diffusion-controlled charge storage kinetics, a peculiar characteristic of pseudocapacitors. It is noteworthy to observe that the diffusion current (%) decreases from 93 to 57% when the scan rate changes from 1 to 100 mV s^{-1}. This is due to the fact that at lower scan rates, the conducting ions have sufficient time to diffuse toward and/or away from the electrode surface, influencing the overall charge storage dynamics.[63]

https://doi.org/10.1021/acsomega.4c06108
ACS Omega 2024, 9, 41807−41818

To further substantiate these conclusions, the b-value was obtained from a plot of $\log(i_p)$ vs $\log(v)$ following the Randles–Ševčik equation (eq 5). A b-value ranging between $0.35 < b < 0.7$ indicates a typical diffusion-limited process.[62] In the present case, the b-value obtained from a linear plot of $\log(i_p)$ vs $\log(v)$ was found to be 0.551 (Figure 6c). This further validates our analysis of Cd(DAB) being an electrode material for intercalated pseudocapacitors. The remarkable pseudocapacitance behavior seen (discussed in further sections) is ascribed to diffusive capacitance from the intercalation and/or deintercalation of conducting ions between the layers of metal–ligand COP.[64,65]

$$i_p = av^b \quad (5)$$

The mechanism of intercalation in pseudocapacitance of Cd(DAB) may involve reversible insertion and extraction of electrolyte ions into the interlayer spaces of the material's structure during the charge–discharge process. This process may be characterized by fast faradaic reactions that occur at the surface and near-surface regions of the electrode material, Cd(DAB). When the SC is charged, ions from the electrolyte intercalate into the layers of Cd(DAB). This intercalation process may be facilitated by the layered nature of Cd(DAB), which provides ample space and pathways for ion movement. The intercalation may lead to a change in the oxidation state of Cd^{2+}, contributing to the overall capacitance through faradaic charge transfer reactions. Upon discharge, these ions may be deintercalated, returning to the electrolyte. This reversible ion intercalation/deintercalation process enables high capacitance and energy density, characteristic of pseudocapacitive materials (Figure S5).

GCD curves help in determining the specific capacity by providing insight into the material's charge–discharge time. Figure 6d displays the GCD curves obtained at varying current densities within the potential window of 0–0.4 V. The shape of GCD curves correlates with the pseudocapacitive behavior of the material. A longer discharge period is achieved at lower current densities. Figure S6 depicts a graph of specific capacitance obtained at different current densities. Based on the curve, the specific capacitance of Cd(DAB) at 1 A g^{-1} is 1341.6 F g^{-1}. Cd(DAB) was found to have an energy density of 29.4 Wh kg^{-1} and a power density of 266.7 W kg^{-1}. Nyquist plot, obtained from EIS data, is depicted in Figure 6e. The electrode materials' charge transfer resistance (R_{ct}) can be found from EIS. This aids in assessing the material's specific capacity. A lower R_{ct} value indicates a high degree of conductivity in the electrode material, which translates into a good energy storage performance. Cd(DAB) shows an R_{ct} value of 24.42 Ω. This suggests that the synthesized COP, Cd(DAB), exhibits semiconducting behavior probably owing to delocalization of electrons across the extended π-conjugation in the proposed layered structure (mobility of charge carriers). Previous reports on specific COPs have also demonstrated their semiconducting properties.[66]

From Figure 6f, it is clear that Cd(DAB) shows 81% capacitive retention over 10,000 charge–discharge cycles. From the FESEM image of the COP after 10,000 cycles, it is clear that there was no disintegration or decomposition of the material; however, a slight change in layered morphology with possible restacking is observed (inset Figure 6f). The retention of the structure of the COP was further confirmed by recording the XRD patterns of the electrode used (Figure S7). The X-ray pattern of the used electrode (blue trace) when compared with that of unused COP (maroon trace) clearly indicates that Cd(DAB) maintains its structural integrity and crystallinity after 10,000 charge–discharge cycles. However, a slight decrease in the intensity of peaks maybe attributed to slight rearrangements of the Cd(DAB) lattice caused by redox reactions and ion intercalation. Additionally, the diffractogram depicts peaks corresponding to Ni, owing to its use as a substrate for preparing the working electrode.

When used as an electrode for pseudocapacitors, the synthesized material Cd(DAB) exhibits a remarkable performance. The specific capacitance of 1341.6 F g^{-1} obtained is superior to that of related Cd-based materials reported in earlier literature, as shown in Table 3. Deka et al. reported the synthesis of a 3D cuboidal-shaped Cd-MOF via a slow diffusion technique. The electroactive MOF demonstrated a specific capacitance of 647 F g^{-1} with an excellent retention capacity of 78% for 10,000 cycles.[67] In another work, a multifunctional MOF with 2-(2,5-dicarboxylphenyl)nicotinic acid as the ligand demonstrated a low capacitance of 321 F g^{-1} with 95% retention after 1000 cycles.[68] Manzoor and co-workers synthesized a nanohybrid ZrO_2/CdS via a coprecipitation technique that showed a flower like morphology.[69] The pseudocapacitive material exhibited a high specific capacitance of 1391 F g^{-1}, which was ascribed to the presence of channels in the flower-like structure aiding in rapid transport of ions. A ternary composite, Cu_2O–CdFe NPs@g-C_3N_4, also has been reported to give nearly similar capacitance values of 1067 F g^{-1}.[72] In other works, Cd@Co_3O_4,[71] CdS,[72] and CdS on nickel foam[73] have been reported to give a capacitance of 737, 854, and 909 F g^{-1}, respectively. Other works involved Sr-doped CdO[74] and CdS-decorated ZIF-8[75] with a specific capacitance of 752 and 1065 F g^{-1}, respectively. As observed from the literature, Cd-based materials have been reported to show appreciable pseudocapacitive behavior, and Cd(DAB) appears to stand out in terms of its charge storage capacity.

Table 3. Summary of Cd-Based Materials Reported for Their Energy Storage Behavior

Sl. no	Material	Specific capacitance (F g^{-1})	Reference
1	Cd-MOF	647	67
2	ZrO_2/CdS	1391	69
3	Cu_2O–CdFe NPs@g-C_3N_4	1067	70
4	$\{[Cd(Hcpnc)(DMF)]DMF{\cdot}2H_2O\}_n$	321	68
5	Cd@Co_3O_4	737	71
6	CdS/NF	909	73
7	CdS	854	72
8	Sr-doped CdO	752	74
9	CdS-decorated ZIF-8	1065	75
10	Cd(DAB)	1341.6	this work

Fabrication of an Asymmetrical Supercapacitor Device Using Cd(DAB). Cd(DAB) was further employed as a current collector to fabricate an asymmetrical SC device, where activated carbon was used as the other electrode in 3 M KOH as electrolyte. Figure 7a depicts the cyclic voltammograms in the potential window 0–1.4 V, with scan rates varying from 100 to 10 mV s^{-1}. The CV curves display an intermediate shape between perfectly rectangular (indicative of pure double-layer capacitance) and sharp, well-defined redox peaks (indicative of strong faradaic reactions). The presence of

https://doi.org/10.1021/acsomega.4c06108
ACS Omega 2024, 9, 41807–41818

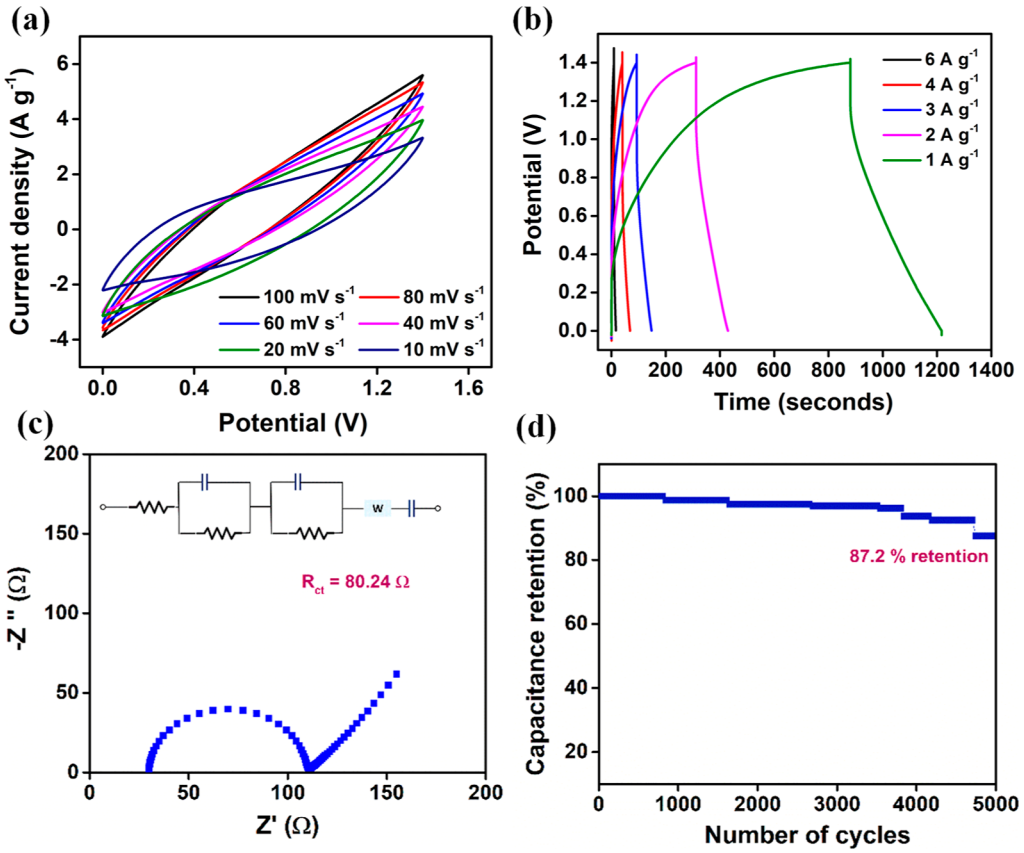

Figure 7. (a) Cyclic voltammograms of Cd(DAB) at various scan rates, (b) GCD curves at different current densities, (c) Nyquist plot, and (d) Cyclic stability of Cd(DAB) at a current density of 6 A g^{-1} using a two-electrode system.

hollow peaks and a degree of symmetry around the zero current axis suggest the pseudocapacitive nature of the electrode material. Essentially, the intermediate shape occurs as a result of activated carbon, which is known to show EDLC-type capacitive behavior.

The GCD curves recorded in a potential window of 0−1.4 V (Figure 7b) showcase a nearly triangular shape, with slight deviations from linearity, thereby reflecting the pseudocapacitive nature of the as-synthesized COP. The specific capacitance of Cd(DAB) in the two-electrode system is estimated to be 428.5 F g^{-1} at a current density of 1 A g^{-1}. The energy density and power density were calculated to be 116.6 Wh kg^{-1} and 1399.2 W kg^{-1}, respectively. The fabricated device shows a R_{ct} of 80.24 Ω, as estimated from EIS (Figure 7c). As seen in Figure 7d, the fabricated device retains 87.2% capacitance after 5000 charge−discharge cycles, indicating its stability. Hence, Cd(DAB) and activated carbon-based asymmetrical SCs exhibit promising electrochemical performance with high specific capacitance, moderate resistance, and excellent stability, making them strong candidates for efficient energy storage solutions.

CONCLUSIONS

The synthesis and characterization of a novel COP derived from the N4 ligand and Cd(II) ions have been presented. The synthetic procedure developed is extremely simple, high yielding, and scalable. The composition and morphology of COP have been thoroughly investigated with the help of standard spectroscopic and microscopic techniques. While the XRD probing verified the crystalline nature, FESEM and HRTEM images corroborated the planar 2D layered structure of the COP. The electrochemical measurements revealed its characteristics for efficient energy storage. In particular, the COP exhibited a specific capacitance of 1341.6 F g^{-1} at 1 A g^{-1} and a stability of 81% capacitance retention after 10,000 cycles at 20 A g^{-1}. Additionally, an asymmetrical SC device was fabricated by using Cd(DAB), which exhibited a specific capacitance of 428.5 F g^{-1} at a current density of 1 A g^{-1}. Moreover, it revealed an excellent energy density and power density of 116.6 Wh kg^{-1} and 1399.2 W kg^{-1}, respectively. In essence, the affordable Cd(DAB) realized in this work has been demonstrated to be an ideal electrode material for energy storage (pseudocapacitor) applications.

ASSOCIATED CONTENT

Supporting Information

The Supporting Information is available free of charge at https://pubs.acs.org/doi/10.1021/acsomega.4c06108.

SEM micrograph with a resolution of 512 × 340, EDS spectrum of Cd(DAB), and elemental mapping showing the presence of C, N, and Cd; thermogram of Cd(DAB); CV curve of Cd(DAB), Cd(DAB), and bare Ni foam, at 10 mV s^{-1}; cyclic voltammograms at lower scan rates (1−10 mV s^{-1}) and plot of $\frac{i_p}{v^{1/2}}$ vs $v^{1/2}$; plausible mechanism for pseudocapacitance in Cd-(DAB); plot of specific capacitance vs current density; and X-ray diffractogram of Cd(DAB) coated on nickel foam after stability test (PDF)

https://doi.org/10.1021/acsomega.4c06108
ACS Omega 2024, 9, 41807−41818

AUTHOR INFORMATION

Corresponding Authors

Sunaja Devi Kalathiparambil Rajendra Pai − *Department of Chemistry, Christ University, Bangalore 560029 Karnataka, India;* orcid.org/0000-0001-7826-1620; Email: sunajadevi.kr@christuniversity.in

Channabasaveshwar V. Yelamaggad − *Centre for Nano and Soft Matter Sciences (CeNS), Bengaluru 562162 Karnataka, India; Department of Chemistry, Manipal Institute of Technology, Manipal Academy of Higher Education, Manipal 576104 Karnataka, India; SJB Institute of Technology, Health & Education City, Bengaluru 560060 Karnataka, India;* Email: cv.yelamaggad@manipal.edu

Authors

Samika Anand − *Department of Chemistry, Christ University, Bangalore 560029 Karnataka, India*

Abhishek Kumar − *Centre for Nano and Soft Matter Sciences (CeNS), Bengaluru 562162 Karnataka, India; Department of Chemistry, Manipal Institute of Technology, Manipal Academy of Higher Education, Manipal 576104 Karnataka, India*

Complete contact information is available at: https://pubs.acs.org/10.1021/acsomega.4c06108

Author Contributions

S.A.: data curation, conceptualization, methodology, investigation, and writing—original draft. S.D.K.R.: supervision, conceptualization, project administration, writing—review and editing, and validation. A.K.: data curation and formal analysis. C.V.Y.: supervision, writing—review and editing, and validation.

Funding

The funds received from Company Young Mind Creations Technologies Pvt Ltd., Bangalore, for article processing charges and membership fee of Channabasaveshwar V Yelamaggad is greatly acknowledged.

Notes

The authors declare no competing financial interest.

ACKNOWLEDGMENTS

The authors acknowledge the support of Central Instrumentation Facility (CIF), Christ University, Bangalore, and Central Research Facility (CRF), Centre for Nano and Soft Matter Sciences (CeNS), Bangalore. Samika Anand is grateful to the Department of Science and Technology, Government of India, for providing INSPIRE fellowship.

REFERENCES

(1) Gür, T. M. Review of Electrical Energy Storage Technologies, Materials and Systems: Challenges and Prospects for Large-Scale Grid Storage. *Energy Environ. Sci.* **2018**, *11* (10), 2696−2767.

(2) Ye, D.; Liu, L.; Peng, Q.; Qiu, J.; Gong, H.; Zhong, A.; Liu, S. Effect of Controlling Thiophene Rings on D-A Polymer Photocatalysts Accessed via Direct Arylation for Hydrogen Production. *Molecules* **2023**, *28* (11), 4507.

(3) Huang, X.-M.; Chen, N.; Ye, D.-N.; Zhong, A.-G.; Liu, H.; Li, Z.; Liu, S.-Y. Structurally Complementary Star-Shaped Unfused Ring Electron Acceptors with Simultaneously Enhanced Device Parameters for Ternary Organic Solar Cells. *Sol. RRL* **2023**, *7* (11), 2300143.

(4) Liu, X.; Yang, H.; Diao, Y.; He, Q.; Lu, C.; Singh, A.; Kumar, A.; Liu, J.; Lan, Q. Recent Advances in the Electrochemical Applications of Ni-Based Metal Organic Frameworks (Ni-MOFs) and Their Derivatives. *Chemosphere* **2022**, *307*, 135729.

(5) Abdel Maksoud, M. I. A.; Fahim, R. A.; Shalan, A. E.; Abd Elkodous, M.; Olojede, S. O.; Osman, A. I.; Farrell, C.; Al-Muhtaseb, A. H.; Awed, A. S.; Ashour, A. H.; Rooney, D. W. Advanced Materials and Technologies for Supercapacitors Used in Energy Conversion and Storage: A Review. *Environ. Chem. Lett.* **2021**, *19* (1), 375−439.

(6) Yadlapalli, R. T.; Alla, R. R.; Kandipati, R.; Kotapati, A. Super Capacitors for Energy Storage: Progress, Applications and Challenges. *J. Energy Storage* **2022**, *49*, 104194.

(7) Jana, S.; Saha, S.; Chandra, A.; El Fallah, S.; Das, S.; Sinha, C. A Cu(II) Metal Organic Framework with a Tetranuclear Core: Structure, Magnetism, and Supercapacitor Activity. *Cryst. Growth Des.* **2022**, *22* (2), 1172−1181.

(8) Chen, B.; Xu, L.; Xie, Z.; Wong, W. Supercapacitor Electrodes Based on Metal-organic Compounds from the First Transition Metal Series. *EcoMat* **2021**, *3* (3), No. e12106.

(9) Abednatanzi, S.; Gohari Derakhshandeh, P.; Depauw, H.; Coudert, F.-X.; Vrielinck, H.; Van Der Voort, P.; Leus, K. Mixed-Metal Metal−Organic Frameworks. *Chem. Soc. Rev.* **2019**, *48* (9), 2535−2565.

(10) Chang, X.-H.; Zhao, Y.; Han, M.-L.; Ma, L.-F.; Wang, L.-Y. Five Cd(Ii) Coordination Polymers Based on 2,3′,5,5′-Biphenyltetracarboxylic Acid and N-Donor Coligands: Syntheses, Structures and Fluorescent Properties. *CrystEngComm* **2014**, *16* (28), 6417−6424.

(11) Liu, J.-Q.; Luo, Z.-D.; Pan, Y.; Kumar Singh, A.; Trivedi, M.; Kumar, A. Recent Developments in Luminescent Coordination Polymers: Designing Strategies, Sensing Application and Theoretical Evidences. *Coord. Chem. Rev.* **2020**, *406*, 213145.

(12) Ghosh, A. K.; Hazra, A.; Mondal, A.; Banerjee, P. Weak Interactions: The Architect behind the Structural Diversity of Coordination Polymer. *Inorg. Chim. Acta* **2019**, *488*, 86−119.

(13) Khrizanforov, M. N.; Zagidullin, A. A.; Shekurov, R. P.; Farida, F.; Bezkishko, I. A.; Ermolaev, V. V.; Miluykov, V. A. Inorganic and Organometallic Polymers as Energy Storage Materials and Enhancing Their Efficiency Inorganic and Organometallic Polymers as Energy Storage. *Comments Inorg. Chem.* **2023**, *00* (00), 1−45.

(14) Behera, N.; Duan, J.; Jin, W.; Kitagawa, S. The Chemistry and Applications of Flexible Porous Coordination Polymers. *EnergyChem* **2021**, *3* (6), 100067.

(15) López-Molino, J.; Amo-Ochoa, P. Gas Sensors Based on Copper-Containing Metal-Organic Frameworks, Coordination Polymers, and Complexes. *ChemPlusChem* **2020**, *85* (7), 1564−1579.

(16) Rahaman, S.; Kanakala, M. B.; Waldiya, M.; Sadhanala, A.; Yelamaggad, C. V.; Pandey, K. Scalable Novel Lanthanide-Ligand Complex for Robust Flexible Micro-Supercapacitors. *J. Power Sources* **2023**, *564* (December 2022), 232801.

(17) Pena, E. S.; Lifshits, L. M.; Eckshtain-Levi, M.; Bachelder, E. M.; Ainslie, K. M. Metal-Organic Coordination Polymers for Delivery of Immunomodulatory Agents, and Infectious Disease and Cancer Vaccines. *WIREs Nanomed. Nanobiotechnol.* **2023**, *15* (4), No. e1877.

(18) Gu, J.; Wen, M.; Cai, Y.; Shi, Z.; Nesterov, D. S.; Kirillova, M. V.; Kirillov, A. M. Cobalt(II) Coordination Polymers Assembled from Unexplored Pyridine-Carboxylic Acids: Structural Diversity and Catalytic Oxidation of Alcohols. *Inorg. Chem.* **2019**, *58* (9), 5875−5885.

(19) Zhao, J.; Dang, Z.; Muddassir, M.; Raza, S.; Zhong, A.; Wang, X.; Jin, J. A New Cd(II)-Based Coordination Polymer for Efficient Photocatalytic Removal of Organic Dyes. *Molecules* **2023**, *28* (19), 6848.

(20) Wang, H.-N.; Meng, X.; Dong, L.-Z.; Chen, Y.; Li, S.-L.; Lan, Y.-Q. Coordination Polymer-Based Conductive Materials: Ionic Conductivity vs. Electronic Conductivity. *J. Mater. Chem. A* **2019**, *7* (42), 24059−24091.

(21) Li, A.-L.; Qu, Y.-H.; Fu, L.; Han, C.; Cui, G.-H. Multidimensional Luminescent Cobalt(Ii)-Coordination Polymers as Sensors with Extremely High Sensitivity and Selectivity for Detection of Acetylacetone, Benzaldehyde and $Cr_2O_7^{2-}$. *CrystEngComm* **2020**, *22* (15), 2656−2666.

(22) Gorai, T.; Schmitt, W.; Gunnlaugsson, T. Highlights of the Development and Application of Luminescent Lanthanide Based Coordination Polymers, MOFs and Functional Nanomaterials. *Dalton Trans.* **2021**, *50* (3), 770−784.
(23) Zhang, X.; Zhang, W.; Xiang, R.; Lan, L.; Dong, X.; Sakiyama, H.; Muddassir, M. Auxiliary Linkers-Induced Assembly of Two 2D Co(II)-Based Coordination Polymers with Different Interpenetrating Fashion: Structure and Magnetism. *Polyhedron* **2023**, *244*, 116625.
(24) Yang, C.; Gu, Y.; Zhang, K.-L. Proton-Conductive and Electrochemical-Sensitive Sensing Behavior of a New Mn(II) Chain Coordination Polymer. *Cryst. Growth Des.* **2023**, *23* (2), 704−718.
(25) Chodankar, N. R.; Pham, H. D.; Nanjundan, A. K.; Fernando, J. F. S.; Jayaramulu, K.; Golberg, D.; Han, Y.; Dubal, D. P. True Meaning of Pseudocapacitors and Their Performance Metrics: Asymmetric versus Hybrid Supercapacitors. *Small* **2020**, *16* (37), 2002806.
(26) Fleischmann, S.; Mitchell, J. B.; Wang, R.; Zhan, C.; Jiang, D.; Presser, V.; Augustyn, V. Pseudocapacitance: From Fundamental Understanding to High Power Energy Storage Materials. *Chem. Rev.* **2020**, *120* (14), 6738−6782.
(27) Hong, Y.; Chen, T.; Wang, K.; Chen, C.; Zhang, C.; Wu, H. Supercapacitive Study for Electrode Materials around the Framework-Collapse Point of a Nibased Coordination Polymer. *CrystEngComm* **2023**, *25*, 122−129.
(28) Tang, L.-P.; Yang, S.; Liu, D.; Wang, C.; Ge, Y.; Tang, L.-M.; Zhou, R.-L.; Zhang, H. Two-Dimensional Porous Coordination Polymers and Nano-Composites for Electrocatalysis and Electrically Conductive Applications. *J. Mater. Chem. A* **2020**, *8* (29), 14356−14383.
(29) Lee, J.-S. M.; Otake, K.; Kitagawa, S. Transport Properties in Porous Coordination Polymers. *Coord. Chem. Rev.* **2020**, *421*, 213447.
(30) Aldwayyan, A. S.; Al-Jekhedab, F. M.; Al-Noaimi, M.; Hammouti, B.; Hadda, T. B.; Suleiman, M.; Warad, I. Synthesis and Characterization of CdO Nanoparticles Starting from Organometalic Dmphen-CdI2 Complex. *Int. J. Electrochem. Sci.* **2013**, *8* (8), 10506−10514.
(31) EL-Saied, F. A.; Shakdofa, M. M. E.; Al-Hakimi, A. N. Synthesis, Characterization and Antimicrobial Activities of Hydrazone Ligands Derived from 2-(Phenylamino)Acetohydrazide and Their Metal Complexes. *J. Korean Chem. Soc.* **2011**, *55* (3), 444−453.
(32) Karabacak, M.; Bilgili, S.; Atac, A. Molecular Structure, Spectroscopic Characterization, HOMO and LUMO Analysis of 3,3′-Diaminobenzidine with DFT Quantum Chemical Calculations. *Spectrochim. Acta, Part A* **2015**, *150* (May), 83−93.
(33) Wu, C.; Dong, L.; Huang, J.; Williams, P. T. Optimising the Sustainability of Crude Bio-Oil via Reforming to Hydrogen and Valuable by-Product Carbon Nanotubes. *RSC Adv.* **2013**, *3* (42), 19239.
(34) Liu, H.; Kuila, T.; Kim, N. H.; Ku, B.-C.; Lee, J. H. In Situ Synthesis of the Reduced Graphene Oxide−Polyethyleneimine Composite and Its Gas Barrier Properties. *J. Mater. Chem. A* **2013**, *1* (11), 3739.
(35) Thapliyal, V.; Alabdulkarim, M. E.; Whelan, D. R.; Mainali, B.; Maxwell, J. L. A Concise Review of the Raman Spectra of Carbon Allotropes. *Diamond Relat. Mater.* **2022**, *127*, 109180.
(36) Friese, V. A.; Kurth, D. G. From Coordination Complexes to Coordination Polymers through Self-Assembly. *Curr. Opin. Colloid Interface Sci.* **2009**, *14* (2), 81−93.
(37) Yang, L.; Yu, Y.; Feng, J.; Wu, J.; Jiang, L.; Dan, Y.; Qiu, Y. Charge Transfer Induced Unexpected Red-Shift Absorption of Zn and Cu Porous Coordination Polymers Based on Electron-Withdrawing Ligand. *J. Photochem. Photobiol., A* **2018**, *350*, 103−110.
(38) Kaeser, A.; Mohankumar, M.; Mohanraj, J.; Monti, F.; Holler, M.; Cid, J.-J.; Moudam, O.; Nierengarten, I.; Karmazin-Brelot, L.; Duhayon, C.; Delavaux-Nicot, B.; Armaroli, N.; Nierengarten, J.-F. Heteroleptic Copper(I) Complexes Prepared from Phenanthroline and Bis-Phosphine Ligands. *Inorg. Chem.* **2013**, *52* (20), 12140−12151.
(39) Solís, R. R.; Gómez-Avilés, A.; Belver, C.; Rodriguez, J. J.; Bedia, J. Microwave-Assisted Synthesis of NH2-MIL-125(Ti) for the Solar Photocatalytic Degradation of Aqueous Emerging Pollutants in Batch and Continuous Tests. *J. Environ. Chem. Eng.* **2021**, *9* (5), 106230.
(40) Lv, H.; Zhang, H.; Ji, G. Development of Novel Graphene/g-C 3 N 4 Composite with Broad-Frequency and Light-Weight Features. *Part. Part. Syst. Charact.* **2016**, *33* (9), 656−663.
(41) Wu, Y.; Wang, H.; Tu, W.; Wu, S.; Chew, J. W. Construction of hole-transported MoO_x coupled with CdS nanospheres for boosting photocatalytic performance via oxygen-defects-mediated Z-scheme charge transfer. *Appl. Organomet. Chem.* **2019**, *33* (4), 1−13.
(42) Park, Y. R.; Jeong, H. Y.; Seo, Y. S.; Choi, W. K.; Hong, Y. J. Quantum-Dot Light-Emitting Diodes with Nitrogen-Doped Carbon Nanodot Hole Transport and Electronic Energy Transfer Layer. *Sci. Rep.* **2017**, *7* (1), 46422.
(43) Khan, W. U.; Wang, D.; Wang, Y. Highly Green Emissive Nitrogen-Doped Carbon Dots with Excellent Thermal Stability for Bioimaging and Solid-State LED. *Inorg. Chem.* **2018**, *57* (24), 15229−15239.
(44) Borsari, M. Cadmium: Coordination Chemistry. In *Encyclopedia of Inorganic and Bioinorganic Chemistry*; Wiley, 2014; pp 1−16.
(45) Ward, M. Applications of Coordination Chemistry. In *Comprehensive Coordination Chemistry*; Wilkinson, G., Gillard, R. D., McCleverty, J. A., Eds.; Elsevier, 1987.
(46) Zhai, Q.-G.; Wu, X.-Y.; Chen, S.-M.; Lu, C.-Z.; Yang, W.-B. Construction of Cd/Zn(II)-1,2,4-Triazolate Coordination Complexes via Changing Substituents and Anions. *Cryst. Growth Des.* **2006**, *6* (9), 2126−2135.
(47) Hoppe, R. The Coordination Number − an "Inorganic Chameleon.". *Angew. Chem., Int. Ed. Engl.* **1970**, *9* (1), 25−34.
(48) Bhat, S. A.; Palakurthy, N. B.; Kambhala, N.; Subramanian, A.; Shankar Rao, D. S.; Krishna Prasad, S.; Yelamaggad, C. V. Gram-Scale Synthesis and Multifunctional Properties of a Two-Dimensional Layered Copper(II) Coordination Polymer. *ACS Appl. Polym. Mater.* **2020**, *2* (4), 1543−1552.
(49) Alex, C.; Bhat, S. A.; John, N. S.; Yelamaggad, C. V. Highly Efficient and Sustained Electrochemical Hydrogen Evolution by Embedded Pd-Nanoparticles on a Coordination Polymer—Reduced Graphene Oxide Composite. *ACS Appl. Energy Mater.* **2019**, *2* (11), 8098−8106.
(50) Hall, G. S.; Soderberg, R. H. Crystal and Molecular Structure of Bis(o-Phenylenediamino)Nickel, Ni[C6H4(NH)2]2. *Inorg. Chem.* **1968**, *7* (11), 2300−2303.
(51) Maxwell, I. E.; Bailey, M. F. Crystal and Molecular Structure of a Nickel(II) Macrocyclic Tetra-Imine Complex: 5,7,7,12,12,14-Hexamethyl-1,4,8,11-Tetra-Azacyclotetradeca-4,8,10,14-Tetraenenickel(II) Perchlorate. *J. Chem. Soc., Dalton Trans.* **1972**, No. 8−9, 935.
(52) Ricciardi, G.; Rosa, A.; Morelli, G.; Lelj, F. On the Synthesis and Characterization of Cu[C6H4(NH)2]2 [C6H4(NH)2 = Semi-Benzoquinonediiminate] as a Donor Precursor of the Semiconducting and Ferromagnetic Cu[C6H4(NH)2]2(I3)1.66 Charge-Transfer Complex. *Polyhedron* **1991**, *10* (9), 955−961.
(53) Masui, H.; Lever, A. B. P.; Dodsworth, E. S. Substituent Effects and Bonding Characteristics in (o-Benzoquinone Diimine)Bis-(Bipyridine)Ruthenium(II) Complexes. *Inorg. Chem.* **1993**, *32* (3), 258−267.
(54) Dugdale, J. S. *Entropy and Its Physical Meaning*; Taylor & Francis, 2018.
(55) Andrić, J. M.; Janjić, G. V.; Ninković, D. B.; Zarić, S. D. The Influence of Water Molecule Coordination to a Metal Ion on Water Hydrogen Bonds. *Phys. Chem. Chem. Phys.* **2012**, *14* (31), 10896.
(56) Li, C.; Zuo, J. Self-Healing Polymers Based on Coordination Bonds. *Adv. Mater.* **2020**, *32* (27), No. e1903762.
(57) Perrot, P. *A to Z of Thermodynamics*; Oxford University Press on Demand, 1998.
(58) Augustyn, V.; Come, J.; Lowe, M. A.; Kim, J. W.; Taberna, P.-L.; Tolbert, S. H.; Abruña, H. D.; Simon, P.; Dunn, B. High-Rate

https://doi.org/10.1021/acsomega.4c06108
ACS Omega 2024, 9, 41807−41818

Electrochemical Energy Storage through Li+ Intercalation Pseudocapacitance. *Nat. Mater.* **2013**, *12* (6), 518−522.
(59) Banda, H.; Dou, J.-H.; Chen, T.; Libretto, N. J.; Chaudhary, M.; Bernard, G. M.; Miller, J. T.; Michaelis, V. K.; Dincă, M. High-Capacitance Pseudocapacitors from Li + Ion Intercalation in Nonporous, Electrically Conductive 2D Coordination Polymers. *J. Am. Chem. Soc.* **2021**, *143* (5), 2285−2292.
(60) Augustyn, V.; Simon, P.; Dunn, B. Pseudocapacitive Oxide Materials for High-Rate Electrochemical Energy Storage. *Energy Environ. Sci.* **2014**, *7* (5), 1597.
(61) Liu, Y.; Jiang, S. P.; Shao, Z. Intercalation Pseudocapacitance in Electrochemical Energy Storage: Recent Advances in Fundamental Understanding and Materials Development. *Mater. Today Adv.* **2020**, *7*, 100072.
(62) Ge, Y.; Xie, X.; Roscher, J.; Holze, R.; Qu, Q. How to Measure and Report the Capacity of Electrochemical Double Layers, Supercapacitors, and Their Electrode Materials. *J. Solid State Electrochem.* **2020**, *24* (11−12), 3215−3230.
(63) Liang, M.; Zhao, M.; Wang, H.; Shen, J.; Song, X. Enhanced Cycling Stability of Hierarchical NiCo 2 S 4 @Ni(OH) 2 @PPy Core−Shell Nanotube Arrays for Aqueous Asymmetric Supercapacitors. *J. Mater. Chem. A* **2018**, *6* (6), 2482−2493.
(64) Kumar, R.; Bag, M. Quantifying Capacitive and Diffusion-Controlled Charge Storage from 3D Bulk to 2D Layered Halide Perovskite-Based Porous Electrodes for Efficient Supercapacitor Applications. *J. Phys. Chem. C* **2021**, *125* (31), 16946−16954.
(65) González-Meza, O. A.; Larios-Durán, E. R.; Gutiérrez-Becerra, A.; Casillas, N.; Escalante, J. I.; Bárcena-Soto, M. Development of a Randles-Ševčík-like Equation to Predict the Peak Current of Cyclic Voltammetry for Solid Metal Hexacyanoferrates. *J. Solid State Electrochem.* **2019**, *23* (11), 3123−3133.
(66) Morritt, G. H.; Michaels, H.; Freitag, M. Coordination Polymers for Emerging Molecular Devices. *Chem. Phys. Rev.* **2022**, *3* (1), 011306.
(67) Deka, R.; Rajak, R.; Kumar, V.; Mobin, S. M. Effect of Electrolytic Cations on a 3D Cd-MOF for Supercapacitive Electrodes. *Inorg. Chem.* **2023**, *62* (7), 3084−3094.
(68) Liu, Q.-Q.; Yue, K.-F.; Weng, X.-J.; Wang, Y.-Y. Luminescence Sensing and Supercapacitor Performances of a New (3, 3)-Connected Cd-MOF. *CrystEngComm* **2019**, *21*, 6186−6195.
(69) Manzoor, S.; Faheem, M.; Usman, M.; Sadaqat, M.; Naeem, M.; Najam-ul-haq, M. Development of Excellent and Novel Flowery Zirconia/Cadmium Sulfide Nanohybrid Electrode: For High Performance Electrochemical Supercapacitor Application. *J. Energy Storage* **2021**, *40* (April), 102718.
(70) Reddy, N. R.; Reddy, P. M.; Mandal, T. K.; Yedluri, A. K.; Joo, S. W. Architecture of Superior Hybrid Electrode by the Composition of Cu2O Nanoflakes, Novel Cadmium Ferrite (CdFe2O4) Nanoparticles, and g-C3N4 Sheets for Symmetric and Asymmetric Supercapacitors. *J. Energy Storage* **2021**, *43*, 103302.
(71) Deng, S.; Xiao, X.; Chen, G.; Wang, L.; Wang, Y. Cd Doped Porous Co 3 O 4 Nanosheets as Electrode Material for High Performance Supercapacitor Application. *Electrochim. Acta* **2016**, *196*, 316−327.
(72) Rathinamala, I.; Babu, I. M.; William, J. J.; Muralidharan, G.; Prithivikumaran, N. CdS Microspheres as Promising Electrode Materials for High Performance Supercapacitors. *Mater. Sci. Semicond. Process.* **2020**, *105*, 104677.
(73) Xu, P.; Liu, J.; Yan, P.; Miao, C.; Ye, K.; Cheng, K.; Yin, J.; Cao, D.; Li, K.; Wang, G. Preparation of Porous Cadmium Sulphide on Nickel Foam: A Novel Electrode Material with Excellent Supercapacitor Performance. *J. Mater. Chem. A* **2016**, *4*, 4920−4928.
(74) Xavier, A. R.; Ravichandran, A. T.; Vijayakumar, S.; Angelin, M. D.; Rajkumar, S.; Merlin, J. P. Synthesis and Characterization of Sr-Doped CdO Nanoplatelets for Supercapacitor Applications. *J. Mater. Sci. Mater. Electron.* **2022**, *33* (11), 8426−8434.
(75) Christin Jenifer, A.; Kanchana, G.; Kathirvel, D.; Siva, V.; Murugan, A. Nanoscale CdS Enwrapped Zeolite-like Zn-MOF Nanocomposite for Advanced Energy Storage Systems. *Mater. Lett.* **2024**, *368*, 136668.

https://doi.org/10.1021/acsomega.4c06108
ACS Omega 2024, 9, 41807−41818